Comprehensive performance analysis of flexible asynchronous AC link under various unbalanced grid voltage conditions

Imdadullah [a], Syed Muhammad Amrr [b], Atif Iqbal [c,*], M.S. Jamil Asghar [d]

[a] Electrical Engineering Section, University Polytechnic, Aligarh Muslim University, Aligarh 202002, India
[b] Department of Electrical Engineering, Indian Institute of Technology Delhi, New Delhi, 110016, India
[c] Department of Electrical Engineering, Qatar University, Doha, 2713, Qatar
[d] Department of Electrical Engineering, ZHCET, Aligarh Muslim University, Aligarh 202002, India

ABSTRACT

A flexible asynchronous AC link (FASAL) system is a technology that interconnects two power system networks operating at the same or different frequencies. The FASAL system is a newly developed technology; therefore, it requires a thorough investigation under different unbalanced grid voltage conditions for better behavioral understanding and appropriate future controller design. In this paper, the FASAL system is analyzed under various symmetrical and asymmetrical unbalanced grid voltage conditions. Moreover, the performance of the back-to-back voltage source converter (VSC) based HVDC link is also analyzed to establish its comparison with the FASAL system under the same conditions. The FASAL and VSC-HVDC systems are modeled in PSCAD/EMTDC software environment. The simulation results illustrate that the FASAL system performance is better under transient as well as steady-state conditions. Furthermore, the reduction in power at the receiving end side is also lesser in the FASAL system. For example, a 10% sag contributes only a 15% dip in power in the FASAL system, whereas VSC-HVDC reports a 30% power dip for the same sag condition.

1. Introduction

The continuous increase in power generation through power electronic-based distributed generation systems and rapidly changing loads, leads to a degradation in the power quality of distribution systems. The modern power system networks and power utilization are becoming more sensitive to power quality (Ismail et al., 2020). Moreover, the modern industry components comprise power electronic devices, smart sensing, and actuating devices. These components are susceptible to system disturbances which cause voltage sag and swell, variations in voltage and frequency, harmonics, unbalance, and other transient interruptions (Omara and Nassar, 2019; Han et al., 2020). Another source of voltage unbalance is the unequal single-phase loads across a three-phase power network at the distribution level. The improper design steps in the single-phase traction and railroad systems also cause a significant unbalance in the three-phase utility system (Von Jouanne and Banerjee, 2001).

Among all types of power quality (PQ) problems, the voltage sag is the most common phenomenon in the electric power system networks. This is one of the serious problems that affect the

power supply to industrial loads. Fault investigation in the power system shows that almost 80% of the PQ problems are caused by voltage sag (Liu et al., 2020; Lim and Dorr, 2000). Normally, a short circuit fault in the power system causes a short duration of grid disturbances called voltage dip (sag). A voltage sag is a reduction in the RMS (root mean square) voltage magnitude ranging from 10% to 90% with a time duration of half-cycle to one minute (Dugan et al., 1996). A serious voltage sag can lead to triggering of the protection system and the disconnection of DGs from the main grid. It certainly leads to the severe active and reactive power shortage. This threatens the stability and reliability of the power system network (Rodriguez et al., 2007). Therefore, how to ride through such abnormal grid conditions poses one of the crucial technical problem that need to be addressed seriously.

One technique to enhance the voltage reliability is implementing a series active compensator such as dynamic voltage restorer (DVR) (Jiang et al., 2019). It is connected in series with a power distribution line or load bus to protect sensitive loads from voltage sag. The performance of DVR depends on its control strategy and circuit design. There are various control strategies for DVRs, reported in Kang et al. (2017), Somayajula and Crow (2015), and references therein. The recent research focuses on the reduction of the injected voltage rating of a DVR (i.e., in-phase compensation) or mitigating the phase jump to restore the load-side voltage to a pre-fault value (i.e., pre-sag compensation) (Tu et al., 2019).

* Corresponding author.
 E-mail addresses: imdadamu@gmail.com (Imdadullah), syedamrr@gmail.com (S.M. Amrr), atif.iqbal@qu.edu.qa (A. Iqbal), sjasghar@gmail.com (M.S.J. Asghar).

Nomenclature

Abbreviation	Description	Abbreviation	Description
AC	Alternating current	BTB	Back-to-back
DC	Direct current	DG	Distributed generation
$DFIM$	Doubly fed induction machine	DVR	Dynamic voltage restorer
$FACTS$	Flexible AC transmission system	$FASAL$	Flexible asynchronous AC link
$HVDC$	High voltage direct current	GEC	General Electric Company
SLG	Single-line-to-ground	LCC	Line-commutated converters
LG	Line-to-ground	LLG	Line-to-line-to-ground
LL	Line-to-line	MMC	Modular multilevel converters
PCC	Point of common-coupling	VFT	Variable frequency transformer
VSC	Voltage source converter	V_{AC}	AC system voltage
S_B	Rated power	$L_1 \& L_2$	AC system Inductance
SCR	Short circuit ratio of AC system	$f_1 \& f_2$	AC system frequencies
$T_1 \& T_2$	Voltage ratios of transformers	T_{KVA}	Transformer rating in kVA
V_{nDC}	Nominal DC voltage	C_{DC}	DC Capacitor
f_s	Switching frequency	X_T	Transformer leakage reactance

The study of voltage sag is also essential for the asynchronous interconnection of electric power grids through various technologies. The grid interconnections offer improved reliability, reduced power interruption, and minimized power generation cost. Therefore, for the interconnection of two power grids, a robust, reliable, and cost-effective connection is necessary. Among various interconnection technologies, the HVDC system is a widely employed technique throughout the globe for asynchronous interconnection (Ufa et al., 2020; Plihal et al., 2019). Another contemporary technology is the variable frequency transformer (VFT), mainly implemented in the USA and Canada (Imdadullah et al., 2020a).

The performance evaluation of the VSC-HVDC system under unbalanced grid voltage conditions has been substantially studied in the literature (Liu et al., 2018; Tang et al., 2019; Shi and Filizadeh, 2019; Fallah et al., 2020). Nowadays, the research emphasizes on the behavior of modular multilevel converters based HVDC system (MMC-HVDC) under unbalanced grid conditions (Wang et al., 2020; Hao et al., 2020). The main advantages of the VSC-HVDC are: (i) its ability to operate into a very weak ac power network, (ii) no requirement for reactive power supply at the converter, (iii) reduced harmonics, and (iv) good controllability (Guo et al., 2012). However, the main limitation of the HVDC system is its inadequate ability to deal with the natural damping without inertia, and its over-current capability is also low. These factors are crucial for ensuring the reliability and stability of power system networks (Wen et al., 2018). Moreover, the VSC-HVDC system needs high capital cost and incurs relatively more losses than LCC-HVDC system. Further, the VSC-HVDC system operates comparably at a lower voltage, and power ratings (Guo et al., 2012).

As mentioned above, another method for asynchronous interconnection is the variable frequency transformer (Dusseault et al., 2004). This technology is developed for short-distance asynchronous interconnection using a huge rotating mass (rotor), which offers inbuilt natural damping potential to damp out the oscillations in the power system network. Further, its substantial thermal time constant offers a large overloading capacity (Merkhouf et al., 2008). However, the literature of VFT system reveals that the symmetrical and asymmetrical grid faults cause large fault currents, massive torque, and power fluctuations in the system. Hence, it threatens the reliability and security of power system networks, and shortens the life of the VFT or even destroys its mechanical components (Chen et al., 2020). To restrict fault currents and to confine the spreading of symmetrical network fault from the faulty side of VFT to the healthy side, a series of dynamic braking resistors (SDBR) is employed (Ambati et al., 2015). Furthermore, to protect the VFT from asymmetrical

network faults, a single-converter-based control scheme has been proposed (Chen et al., 2020). This scheme can reserve the function of power decoupling control and mitigate the torque and power fluctuations (Chen et al., 2020). However, a very high power DC motor and its drive are needed for the forced rotation of the VFT rotor during severe fault conditions. Furthermore, the VFT system requires a regular shutdown and maintenance due to the replacement of carbon brushes of the DC motor (Marken et al., 2008).

Alternatively, a newly developed technology called flexible asynchronous AC link (FASAL) system can also be employed for asynchronous interconnection between two power system networks working at different operating conditions (Asghar and Imdadullah, 2018; Imdadullah et al., 2019, 2020b). In Imdadullah et al. (2020b), the performance and reliability of the FASAL system is evaluated and compared with the LCC-HVDC link under various fault conditions such as LG, LLG, and LL. It was reported that the FASAL system possesses better steady-state and transient response under fault conditions, than the LCC-HVDC system. However, in the aforementioned work on the FASAL system, the effect of unbalanced grid voltage conditions has not been addressed. The FASAL system's behavior under unbalanced conditions will help better understand the system performance. This will further assist in proposing an appropriate control strategy to deal with such a phenomenon.

Therefore, this paper focuses on analyzing and understanding the FASAL system under various voltage sag conditions. Moreover, to comprehend the effect of unbalanced conditions, the VSC-HVDC system is also analyzed and compared with the FASAL system. Hence, these performances shall help in the future development of a suitable control methodology for the FASAL system, to ride through the grid faults or unbalanced network conditions. The key contributions of this paper are stated below:

- The newly developed FASAL system is investigated under various voltage sag conditions of the power system network, to analyze its behavior.
- The performance of the FASAL system under the influence of symmetrical and asymmetrical unbalanced network conditions is realized in PSCAD/EMTDC software environment.
- The performance of the VSC-HVDC system is also analyzed to substantiate the better performance of the FASAL system under unbalanced grid conditions.
- The effects of various symmetrical and asymmetrical voltage sag conditions are realized to comprehend the system performance in a broader spectrum. Therefore, the symmetrical voltage sag with the magnitude of 10%, 20%, and 30% is taken. Whereas, asymmetrical voltage sag of type C, D, and F are considered.
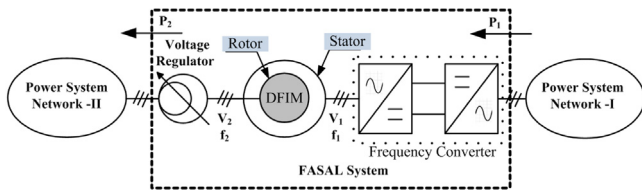
Fig. 1. Interconnection of power system networks through FASAL system.

- The simulation results demonstrate that the FASAL system is achieving a better response under unbalanced grid conditions than the VSC-HVDC system in terms of fewer oscillations, low overshoot, less real power reduction, and lesser reactive power requirement.

The remaining part of this paper is organized as follows. In Section 2, a brief model description of the FASAL system and VSC-HVDC system are presented. In Section 3, the characteristics and classification of voltage sag are presented. In Section 4, analysis of the FASAL and BTB VSC-HVDC systems under symmetrical voltage sag conditions are presented. Moreover, the comparative summary of both the systems under unbalanced network conditions is also reported. In Section 5, the FASAL system response under asymmetrical voltage sag of type C, D and F is realized. Finally, in Section 6, the conclusion of the paper is presented.

2. Brief overview of FASAL system and VSC-HVDC system

In this section, a brief model description of the FASAL system and VSC-HVDC system are presented.

2.1. FASAL system

The FASAL system is used for an asynchronous interconnection between two electric power system networks operating at the same or different frequencies (Asghar and Imdadullah, 2018; Imdadullah et al., 2019, 2020b). It consists of a doubly-fed induction machine (DFIM), voltage regulator and frequency converters as shown in Fig. 1. A power system network-I is connected to the stator through a frequency converter, and power system network-II is connected to the rotor through a voltage regulator. Power transfer takes place from a high-frequency power system network to the low-frequency power system network. The magnitude and direction of power flow are regulated by controlling the voltage and frequency.

The effect of three-phase faults (LLL and LLLG) through the FASAL system is transmitted minimally to the other side of the grid. During this fault condition, the rotor circuit of DFIM gets short-circuited and operates as a typical induction motor. As a result, no significant power transmission occurs from the healthy side to the faulty side of the grid. As a matter of fact, for the acceleration of DFIM, additional limited power is required from the healthy side. During this period, the switchgear will have enough cushion time to operate, i.e., isolating the fault area and localizing the fault (Imdadullah et al., 2019). The FASAL system under fault conditions exhibits better performance.

The mathematical modeling is briefly discussed below. For approximate analysis of DFIM, the magnetizing impedance Z_m is neglected due to its very high value. The simplified expressions of stator and rotor real and reactive powers P_1, P_2 and Q_1, Q_2 are derived accordingly. The apparent power S_1 on the stator side is given by

$$S_1 = P_1 + jQ_1 = V_1 * I_1^* \tag{1}$$

$$= \left[\frac{R(V_1 - \frac{V_2}{s}\cos\delta) - X\frac{V_2}{s}\sin\delta}{R^2 + X^2} \right] V_1$$

$$+ j\left[\frac{X(V_1 - \frac{V_2}{s}\cos\delta) + R\frac{V_2}{s}\sin\delta}{R^2 + X^2} \right] V_1 \tag{2}$$

Thus, the real power (P_1) and reactive power (Q_1) at the stator side are Imdadullah and Asghar (2019):

$$P_1 = \left[X\frac{V_2}{s}\sin\delta - R(V_1 - \frac{V_2}{s}\cos\delta) \right] \left(-\frac{V_1}{Z^2} \right) \tag{3}$$

$$Q_1 = \left[R\frac{V_2}{s}\sin\delta + X(V_1 - \frac{V_2}{s}\cos\delta) \right] \left(\frac{V_1}{Z^2} \right) \tag{4}$$

where $Z = R + jX$

The apparent power S_2 on the rotor side is given by Imdadullah and Asghar (2019):

$$S_2 = P_2 + jQ_2 = \left(\frac{V_2\angle\delta}{s} \right) I_2^* \tag{5}$$

From (5), the rotor apparent power S_2 is given by

$$S_2 = P_2 + jQ_2 = \left(\frac{V_2}{s}\cos\delta + j\frac{V_2}{s}\sin\delta \right) * I_2^*$$

$$= \left[\frac{R\frac{V_2^2}{s^2} + V_1\frac{V_2}{s}(X\sin\delta - R\cos\delta)}{R^2 + X^2} \right]$$

$$+ j\left[\frac{X\frac{V_2^2}{s^2} - V_1\frac{V_2}{s}(X\cos\delta + R\sin\delta)}{R^2 + X^2} \right] \tag{6}$$

Therefore, the rotor real and reactive power at rotor side are Imdadullah and Asghar (2019):

$$P_2 = \left[R\frac{V_2}{s} + V_1(X\sin\delta - R\cos\delta) \right] \left(\frac{V_2}{sZ^2} \right) \tag{7}$$

$$Q_2 = \left[X\frac{V_2}{s} - V_1(X\cos\delta + R\sin\delta) \right] \left(\frac{V_2}{sZ^2} \right) \tag{8}$$

where $s = f_2/f_1$, and the value of R and X is given as:

$$R = R_1 + \frac{R_2}{s}, \quad X = X_1 + X_2. \tag{9}$$

It is evident from the above expressions (3) and (7) that the real power depends on the voltage (V_2) and the frequency (f_1). Therefore, by regulating the values of V_2 and f_1, the FASAL system transfers the power from one side power system network to another.

The advantages of the FASAL system over the HVDC system are: (i) The presence of a large rotating inertial mass in the FASAL system enables it to damp out the oscillations in the power system naturally. (ii) Since the main path of power flow in the FASAL system is free from power electronic converters, it operates smoothly without any harmonics. (iii) The large thermal time constant allows the FASAL system to have higher overloading capacity. (iv) The footprint of the FASAL system is small due to the high power density and non-use of harmonic filters. (v) The slow system dynamics prohibits the interference of the controller with other parts of the system. Thus, the control actuation does not interfere with the neighboring accessories (Imdadullah et al., 2019, 2020b).

2.2. VSC-HVDC system

The HVDC link consists of two voltage source converters (VSCs) (VSC-1 and VSC-2) connected back-to-back through a common DC link. In this case, both the VSCs are three-phase and

Table 1
Recent VSC Projects around the globe.

Project name	Year	Voltage (kV)	Power (MW)	Distance (km)	Remarks (if any)
SydV̀astl̀anken (Sweden–Norway)	2015	400	1200	190	–
HVDC NordBalt (Sweden–Lithuania)	2015	300	700	450	–
Skagerrak 4 (Denmark–Norway)	2015	500	700	244	–
DolWin2 (Germany)	2016	320	900	135	–
Zhoushan (China)	2016	±200	400/300/100 /100/100	5 MT	DC CBs installed
Yu-E (China) Yu (Chongqing) - E (Hubei)	2017	±420	4 × 1250	BTB	Two off two pair in parallel
Zhangbei-1 (China)	2018	±500	3000/3000/ 1500/1500	4 MT DCG	First DC grid project in China
Zhangbei-2 (China)	2020	±500	3000/3000/ 1500/1520	4 MT DCG	–
ALEGrO Interconnector (Germany–Belgium)	2020	320	1000 MW	90	First power bridge between the countries, underground cable

Table 2
ABC classification of three-phase voltage sag types.

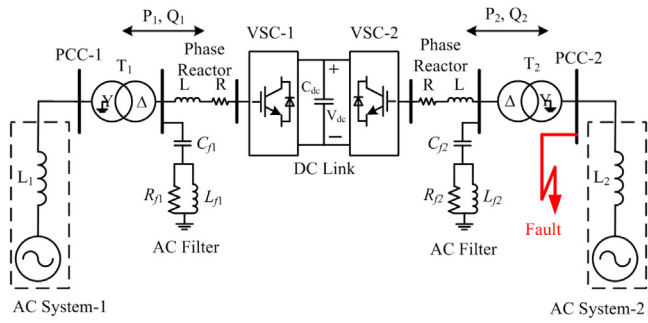| Type	Voltage expressions	Phasor diagram
A	$\bar{E}_A = hE$ $\bar{E}_B = -\frac{1}{2}hE - j\frac{\sqrt{3}}{2}hE$ $\bar{E}_C = -\frac{1}{2}hE + j\frac{\sqrt{3}}{2}hE$	
B	$\bar{E}_A = hE$ $\bar{E}_B = -\frac{1}{2}E - j\frac{\sqrt{3}}{2}E$ $\bar{E}_C = -\frac{1}{2}E + j\frac{\sqrt{3}}{2}E$	
C	$\bar{E}_A = E$ $\bar{E}_B = -\frac{1}{2}E - j\frac{\sqrt{3}}{2}hE$ $\bar{E}_C = -\frac{1}{2}E + j\frac{\sqrt{3}}{2}hE$	
D	$\bar{E}_A = hE$ $\bar{E}_B = -\frac{1}{2}hE - j\frac{\sqrt{3}}{2}E$ $\bar{E}_C = -\frac{1}{2}hE + j\frac{\sqrt{3}}{2}E$	
E	$\bar{E}_A = E$ $\bar{E}_B = -\frac{1}{2}hE - j\frac{\sqrt{3}}{2}hE$ $\bar{E}_C = -\frac{1}{2}hE + j\frac{\sqrt{3}}{2}hE$	
F	$\bar{E}_A = hE$ $\bar{E}_B = -\frac{1}{2}hE - j\frac{1}{\sqrt{12}}(2+h)E$ $\bar{E}_C = -\frac{1}{2}hE + j\frac{1}{\sqrt{12}}(2+h)E$	
G	$\bar{E}_A = \frac{1}{3}(2+h)E$ $\bar{E}_B = -\frac{1}{6}(2+h)E - j\frac{\sqrt{3}}{2}hE$ $\bar{E}_C = -\frac{1}{6}(2+h)E + j\frac{\sqrt{3}}{2}hE$	

Fig. 2. A typical simplified diagram of a BTB VSC–HVDC system.

Fig. 3. Configuration of FASAL system under unbalanced network conditions.

six-pulse IGBT based converters. A general BTB VSC–HVDC system is represented by Fig. 2 (Saeedifard and Iravani, 2010). These converters are interfaced to the grid or AC system through phase reactors and normal power transformers. The use of the reactors reduces the high-frequency harmonic contents of the AC line current. These reactors also control the real and reactive power transmission by controlling the current flow through them. The high-frequency switching ripples present in the AC voltage and current are mitigated by tuned-shunt filters. The DC capacitors supply energy to sustain the power balance during transient conditions and mitigate the ripple in voltage at the DC side. A list of recent VSC projects around the globe is presented in Table 1.

Under a balanced network condition, negative-sequence components are not present. However, the variables such as the voltage and current are only positive-sequence components presented in the positive-sequence reference frame. The ac side system can be formulated in the synchronous d–q reference frame as Eq. (10), where the d-axis is set to the source voltage (Wei and Tang, 2006):

$$\frac{di_{sd}}{dt} = -\frac{R}{L}i_{sd} + \omega i_{sq} + \frac{v_{sd} - v_{cd}}{L}, \tag{10a}$$

$$\frac{di_{sq}}{dt} = -\frac{R}{L}i_{sq} - \omega i_{sd} + \frac{v_{sq} - v_{cq}}{L}. \tag{10b}$$

According to the power balance equation, the dc side system is expressed as:

$$P_{ac} = \frac{3}{2}\left(v_{cd}.i_{sd} + v_{cq}.i_{sq}\right), \tag{11}$$

$$P_{dc} = I_{dc}.V_{dc} + C\frac{dV_{dc}}{dt}.V_{dc},$$

$$= \frac{3}{2}\left(v_{cd}.i_{sd} + v_{cq}.i_{sq}\right). \tag{12}$$

Therefore, Eqs. (10) and (12) represents the one end of VSC-HVDC system under balanced ac network conditions.

3. Characteristics and voltage sag classification

As shown in Fig. 3, it is considered that the power transfer is taking place from power systems network-I (Grid-1) to power systems network-II (Grid-2). Due to the occurrence of a fault, the FASAL system interconnecting the two power system networks will encounter a voltage sag condition. The scope of this section is the characterization and classification of the voltage sags generated by several faults in the power system network.

3.1. Symmetrical sag and Phase-angle jump

In the balanced or symmetrical voltage sag, the voltage dip of the individual phase voltage is equal. This type of sag appears
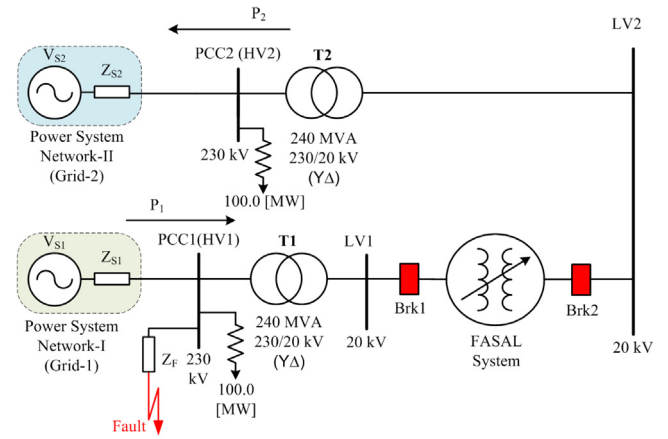
due to three-phase-to-ground fault or the start of a large motor, which is characterized as Type-A sag. The phasor diagram and corresponding voltage expressions of type A sag is shown in Table 2. The magnitude of the sag is denoted by $h \in [0, 1]$. The voltage sag conditions caused by the three-phase fault in the system are formulated by the voltage-divider model, as depicted in Fig. 3. In this figure, the transformers T1 and T2 are used to make the FASAL system compatible with the power system network (grid) voltages. The voltage at the point of common coupling (PCC1), i.e., at the HV side of the transformer T1, can be written as:

$$\bar{V}_{sag} = \left(\frac{\bar{Z}_{F1}}{\bar{Z}_{F1} + \bar{Z}_{S1}}\right).\bar{V}_{S1} \tag{13}$$

where $\bar{V}_{S1}$, $\bar{Z}_{S1}$, and $\bar{Z}_{F1}$ are the pre-fault voltage, the source impedance at PCC1, and the impedance between PCC1 and fault location, respectively.

In general, the three-phase sags are characterized by the remnant voltage magnitude and the time duration. Moreover, a three-phase fault causes a drop in the magnitude of voltages and variation in the phase angles, provided that the X/R ratios of Z_{S1} and Z_{F1} are different. This variation in phase-angle is called "*phase-angle jump*" which is mathematically expressed as:

$$\phi = \arg(\bar{V}_{sag}) = \arg(\bar{Z}_{F1}) - \arg(\bar{Z}_{F1} + \bar{Z}_{S1}), \tag{14}$$

where $\bar{Z}_{S1} = R_{S1} + jX_{S1}$, and $\bar{Z}_{F1} = R_{F1} + jX_{F1}$. So, Eq. (14) can be rewritten as:

$$\phi = \arctan\left(\frac{X_{F1}}{R_{F1}}\right) - \arctan\left(\frac{X_{S1} + X_{F1}}{R_{S1} + R_{F1}}\right). \tag{15}$$

If $\left(\frac{X_{S1}}{R_{S1}}\right)$ is equal to $\left(\frac{X_{F1}}{R_{F1}}\right)$, then (15) becomes zero and there is no phase-angle jump. The following equation can be written using Eq. (14) as

$$\frac{\bar{Z}_{F1}}{\bar{Z}_{S1}} = \lambda \ \exp(j\alpha). \tag{16}$$

The value of λ depends on the fault distance and α is constant for any combination of source impedance and fault impedance. The parameter α is called the impedance angle, which is expressed as:

$$\alpha = \arctan\left(\frac{X_{F1}}{R_{F1}}\right) - \arctan\left(\frac{X_{S1}}{R_{S1}}\right). \tag{17}$$

The variation of phase-angle jump with respect to the sag magnitude for a particular impedance angle is shown in Fig. 4. The graph is plotted for multiple impedance angles, i.e., $+10°$, $0°$,
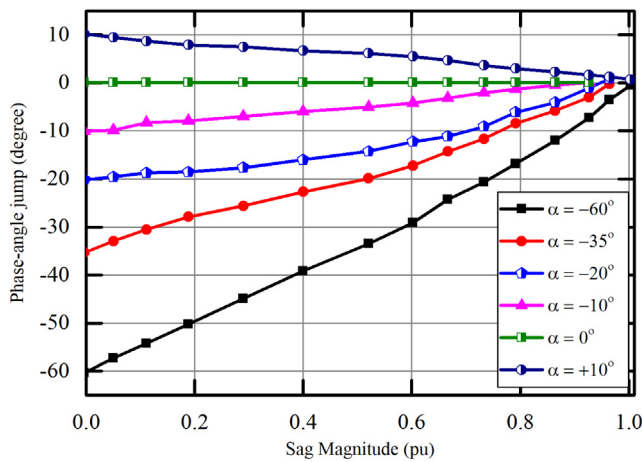
Fig. 4. Variation of phase-angle jump with respect to the sag magnitude for various impedance angles under three-phase faults.

Table 3
Voltage sag transformation in the interconnected power system networks.

Fault Types	Sag at PCC1 (Actual sag occurred)	Sag at Bus LV1 (Trans. Config. YΔ)	Sag at PCC2 (Trans. Config. YΔ)
LLL	Type A	Type A	Type A
LLLG	Type A	Type A	Type A
LL	Type C	Type D	Type C
LLG	Type E	Type F	Type G
LG	Type B	Type C[a]	Type D[a]

[a]The sag magnitude is not equal to V_{sag} but equal to $(1/3+2/3\ V_{sag})$.

−10°, −20°, −35° and −60°. All three-phases are subjected to the equal variation in magnitude and phase-angle under three-phase fault. The relationship depicted in Fig. 4 is also applicable for single-phase equipment.

3.2. Classification of asymmetrical sag

If the dip in the magnitude of individual phase voltages are different or the phase angle between them is other than 120°, the sag is called unbalanced or asymmetrical sag. The causes of asymmetrical sags are the occurrence of asymmetrical faults in the power system network (Mohseni et al., 2011). The fault types include a single-line-to-ground (SLG) fault, line-to-line (LL) fault, or double-line-to-ground (LLG) fault and due to lightning, etc. There are six types of asymmetrical sag, including types B to G, that can arise at the PCC-1.

The phasor diagram and the corresponding voltage equations of different sag types are presented in Table 2. It has been discussed in detail in Bollen (2000), that the connection of transformers cannot influence the voltage sag produced by type A sag. It propagates unaltered throughout the interconnected power system network from the PCC1 (HV1) toward Bus LV1 and PCC2 (HV2) in the system presented in Fig. 3.

The voltage sag appeared at the terminals of the FASAL during asymmetrical faults is significantly distinct from the PCC-1, because of the transformer's connection. The zero-sequence component is filtered out in the secondary side of the transformer, T2, due to its YΔ connection (Bus LV1 in Fig. 3). Table 3 shows that the voltage sag transformation in the interconnected power system networks. It is clear from Table 3 that the sag types B and E cannot reach the terminals of the FASAL system as they include zero-sequence components. This implies that the FASAL system will experience only the sag types A, C, D, and F under any faults listed in Table 3.

4. Analysis of FASAL and VSC-HVDC link under Symmetrical voltage sag

In this section, the performance of the FASAL system is evaluated under the influence of unbalanced network voltage. In these conditions, a small negative-sequence voltage may cause a large negative-sequence current as the negative-sequence impedance of the DFIM is small (Xu et al., 2018). Moreover, due to the presence of negative-sequence components in the network voltage, the stator of DFIM has also a negative-sequence current component. This leads to the fluctuations in the rotor current and electromagnetic torque and reduces the active power. This study provides a better understanding of the FASAL system under symmetrical unbalance conditions. Furthermore, the comparison with the VSC-HVDC system under the same scenario in the next subsection also enables us to justify the selection of the FASAL system as a better alternative for asynchronous interconnection. It also encourages the researcher for its future controller design.

4.1. FASAL system under symmetrical sag conditions

The FASAL system is modeled according to Fig. 3 in the PSCAD/EMTDC software environment and its design parameters are taken from Imdadullah et al. (2019). The transient response of this simulated model under the sag of 10%, 20%, and 30% in network voltage is shown in Fig. 5. These voltage dips are appearing at $t = 4.05$ s in each case. It is well known that the important parameters during sag conditions are the stator voltage, the rotor current, and active power (Gomis-Bellmunt et al., 2008). Therefore, the given simulation study focuses on the observation of these parameters (stator current, the rotor current and the active power) under an unbalancing condition.

It is evident from Fig. 5(a), 5(e), and 5(i) that at $t = 4.05$s, the magnitude of voltages at the grid side decreases due to the symmetrical sag in each case. As a result, the stator current gets distorted, which is depicted in Fig. 5(b), 5(f), and 5(j). Moreover, under type A sag, the unbalanced oscillations in rotor current can be seen in Fig. 5(c), 5(k), and 5(c) corresponding to respective sag conditions. The generation of unbalanced oscillation in the rotor current is due to the natural response of the stator flux throughout the three-phase fault condition.

Furthermore, the voltage dip also causes reduction in the real power production. Before occurrence of any voltage dip, the output of real power was $P_1 = 230$ MW and $P_2 = 192$ MW. However, after the incidence of symmetrical sag, the real power output obtained in each cases are as follows: (i) $P_1 = 188.79$ MW and $P_2 = 156.51$ MW under 10% sag, (ii) $P_1 = 160$ MW and $P_2 = 130$ MW under 20% sag, and (iii) $P_1 = 114.84$ MW and $P_2 = 100.89$ MW under 30% sag. The characteristic behavior of voltage dip level versus real power output P_1 and P_2 is shown in Fig. 6. It is evident from the trajectories of P_1 and P_2 that the power transfer is directly dependent upon the symmetrical voltage dip. The magnitude of real power decreases with the increase in the magnitude of symmetrical voltage sag.

4.2. Analysis of VSC-HVDC system

The simulation model of the VSC-HVDC system is developed based on Fig. 2 using PSCAD/EMTDC software. The parameters of the VSC-HVDC system for the simulation study are chosen according to Table 4 (Saeedifard et al., 2009). The performance VSC-HVDC system is tested under balanced and unbalanced grid conditions to study the performance differences.
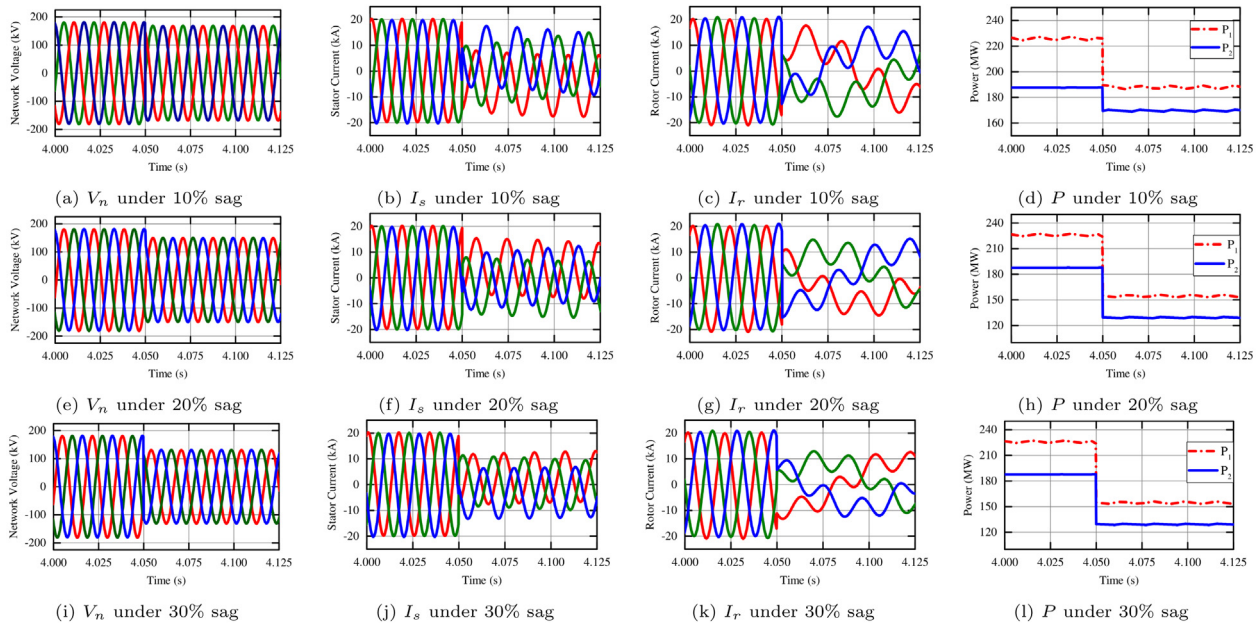
Fig. 5. FASAL system response under symmetrical dip in the network voltage. (i) 10% sag (a)–(d), (ii) 20% sag (e)–(h), and (iii) 30% sag (i)–(l).

Table 4
The main parameters of VSC-HVDC system.

Parameters	Value	Parameters	Value
S_B	110 MVA	T_{KVA}	110 MVA
V_{AC}	138 kV	X_T	5%
L_1&L_2	150 mH	R & L	0.03 Ω, 5 mH
SCR	5	V_{nDC}	60 kV
f_1&f_2	60 Hz	C_{DC}	4000 μF
T_1&T_2	138 kV/30 kV	f_s	2000 Hz

Table 5
VSC-HVDC system under balanced conditions.

Parameters (in pu)	Balanced condition	
	Rectifier	Inverter
V_{DC}	0.998	0.990
I_{DC}	1.00	1.00
P	0.998	0.990
Q	−0.20	−0.10

4.2.1. VSC-HVDC system under balanced network condition

In this system, the real power flows from AC system-1 to AC system-2 and VSC-1 serves as a rectifier while VSC-2 operates as an inverter (Fig. 2). The responses at both ends of the HVDC system is measured in terms of AC voltage (RMS), DC voltage, DC current, real powers, and reactive power. These observations under balanced conditions are shown in Fig. 7.

Initially, at the starting of power transfer, the rectifier DC voltage, DC current, and active reactive observes few oscillations and few overshoot in its transient response, as depicted in Figs. 7(c) and 7(e). These initial inherent transient oscillations are due to the switching phenomenon and not because of voltage sag, and the dedicated control systems (Guo and Zhao, 2009), can tackle them. After 0.7s, these responses settle down to the respective

Fig. 6. Variation of real power transfer under symmetrical voltage dip.

nominal values. On the receiving side, the parameters of VSC-2 (AC voltage, V_{DC}, I_{DC}, P_2, and Q_2) reaches to the steady-state value after 0.8 s, as shown in Figs. 7(b), 7(d), and 7(f). The measurements of VSC-1 and VSC-2 under balanced conditions are presented in Table 5. These observations will help in comparing the performance of the VSC-HVDC system under unbalanced conditions, which is the topic of discussion for the next section.

4.2.2. VSC-HVDC system under unbalanced network conditions

The performance of VSC-HVDC under symmetrical voltage sag of different magnitude, i.e., 10%, 20%, and 30%, is evaluated in this subsection to compare it with the FASAL system. In the simulation analysis, the effect of voltage sag on the AC system-2 is evaluated by observing the performance of DC voltage (V_{DC}), DC current (I_{DC}), and real (P_1, P_2) & reactive (Q_1, Q_2) power exchange between the interconnected networks. The response of these performance parameters under 10%, 20%, and 30% of voltage sag are shown in Figs. 8, 9, and 10, respectively. Moreover, the measurements of these performances are summarized in Table 6.

In view of Figs. 8–10, and Table 6, the following remarks can be made.

(i) The voltage sag appears at the receiving end (inverter side) due to which its performance gets altered. Owing to symmetrical sag, the AC voltage on the inverter side dips down to a lower value (see Figs. 8(b), 9(b), and 10(b)). The transient response of DC voltage and DC current in Figs. 8(d), 9(d), and 10(d) demonstrate that the inverter side gets severely affected due to high overshoot and oscillations. Moreover, the active and reactive powers (P_2, Q_2) also falls down due to the voltage sag (Figs. 8(f), 9(f), 10(f)).
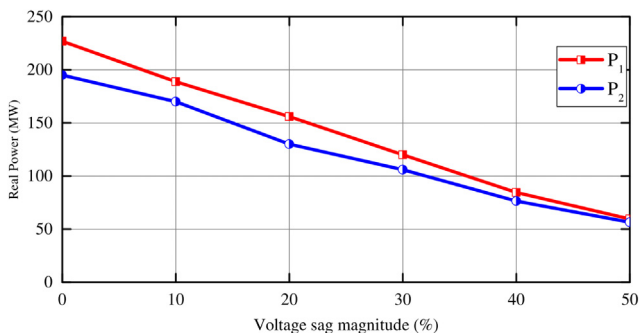
(a) Rectifier side V_{AC}. (b) Inverter side V_{AC}. (c) Rectifier side V_{DC} & I_{DC}.

(d) Inverter side V_{DC} & I_{DC}. (e) Rectifier side P_1 & Q_1. (f) Inverter side P_2 & Q_2.

Fig. 7. VSC-HVDC response under balanced network condition.

(a) Rectifier side V_{AC}. (b) Inverter side V_{AC}. (c) Rectifier side V_{DC} & I_{DC}.

(d) Inverter side V_{DC} & I_{DC}. (e) Rectifier side P_1 & Q_1. (f) Inverter side P_2 & Q_2.
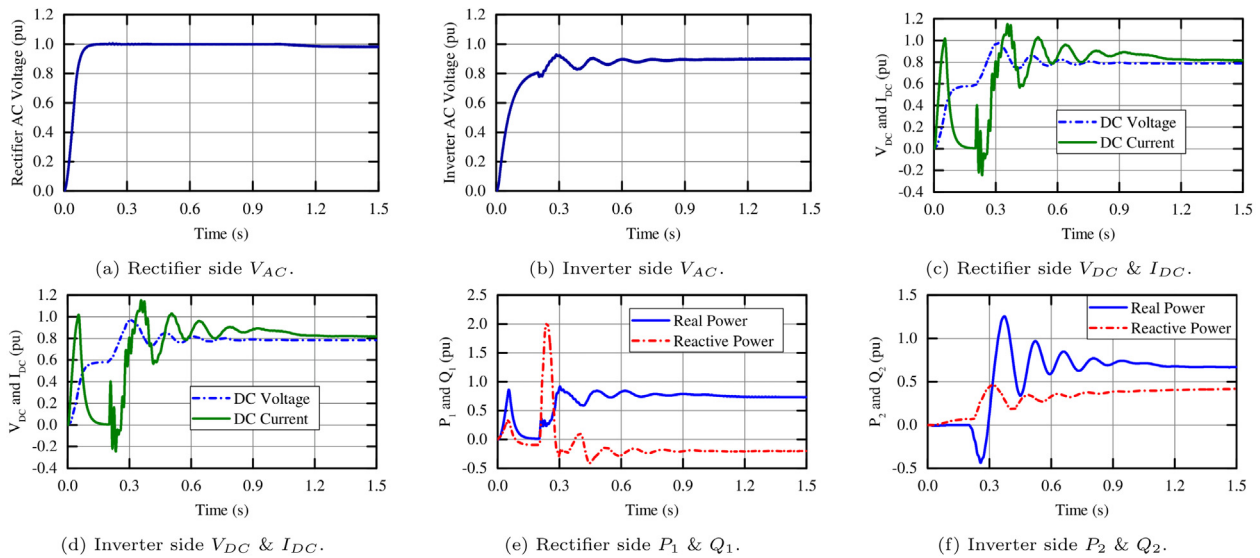
Fig. 8. VSC-HVDC response under 10% symmetrical dip in the network voltage.

(ii) The impact of voltage sag at the VSC-2 is also reflected at the sending end (VSC-1). The DC voltage and DC current on the rectifier side experiences high oscillations and large overshoot value. These oscillations settle down to a new reduced value, after some time, as shown in Table 6. The response of V_{DC} and I_{DC} for each case is shown in Figs. 8(c), 9(c), and 10(c).

(iii) Moreover, the active power also experiences a sudden rise and high oscillation in its value. Similarly, overshoots and oscillations appear in reactive power (Q_1) as shown in Figs. 8(e), 9(e), and 10(e).

The overall performance comparison between the FASAL and HVDC systems under symmetrical sag conditions are presented in the subsequent section.

4.3. Comparison of FASAL system with VSC-HVDC system

Table 7 illustrates a detailed performance comparison between the FASAL system and the BTB VSC-HVDC system under unbalanced network conditions.

Moreover, the reduction in real power due to voltage sag in FASAL and HVDC systems is shown via a bar chart in Fig. 11. It is evident from this plot that at every sag condition, the power reduction under the FASAL system is lesser than the HVDC system, which implies the better performance of FASAL system.

Therefore, it is evident from Table 7 and Fig. 11 that the FASAL system exhibit a better response under unbalanced network conditions due to the natural damping ability (because of the presence of large rotating mass) than the BTB VSC-HVDC link. Thus, the FASAL system provides a better alternative for the interconnection of power system networks while achieving a decent steady-state and transient performance.

5. FASAL system under asymmetrical sag conditions

In this section, simulation analysis has been carried out to evaluate the performance of the FASAL system under various types of asymmetrical voltage sag conditions. It is already mentioned that only sag type C, D, and F are reaching to the FASAL terminals. Therefore, the influence of these sags on the performance of the FASAL system is studied.
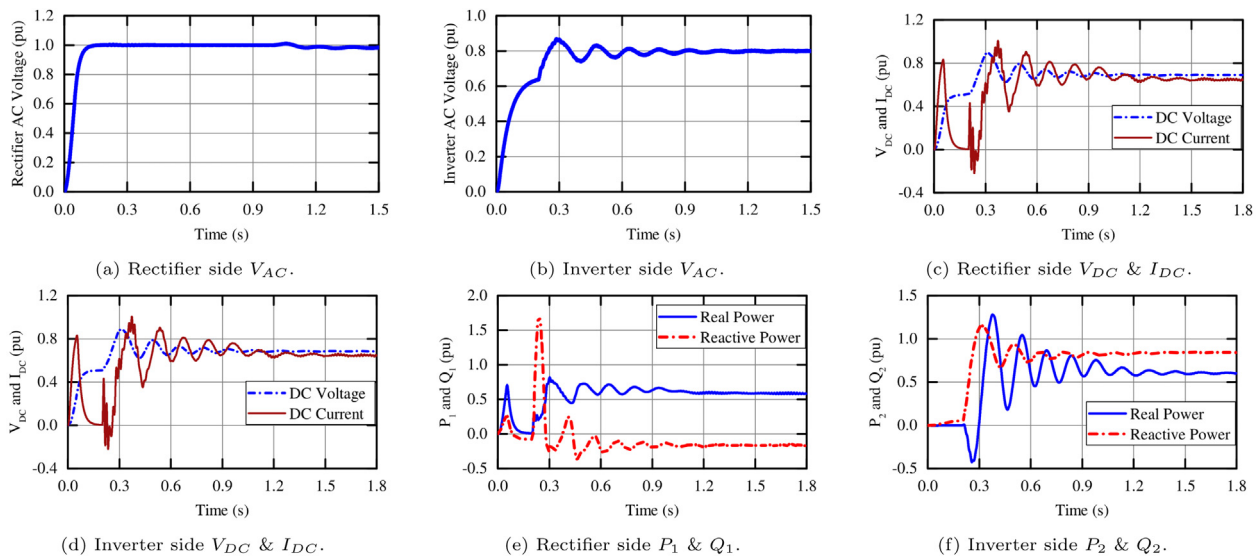
(a) Rectifier side V_{AC}.

(b) Inverter side V_{AC}.

(c) Rectifier side V_{DC} & I_{DC}.

(d) Inverter side V_{DC} & I_{DC}.

(e) Rectifier side P_1 & Q_1.

(f) Inverter side P_2 & Q_2.

Fig. 9. VSC-HVDC response under 20% symmetrical dip in the network voltage.

(a) Rectifier side V_{AC}.

(b) Inverter side V_{AC}.

(c) Rectifier side V_{DC} & I_{DC}.

(d) Inverter side V_{DC} & I_{DC}.

(e) Rectifier side P_1 & Q_1.

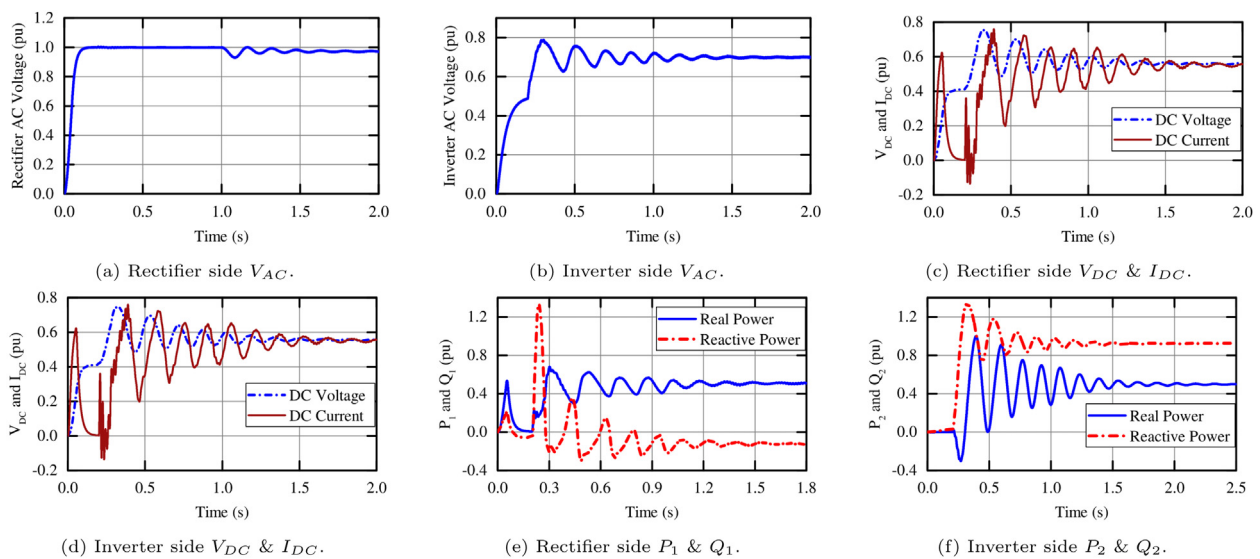(f) Inverter side P_2 & Q_2.

Fig. 10. VSC-HVDC response under 30% symmetrical dip in the network voltage.

Table 6
Performance of the VSC-HVDC system under symmetrical unbalance network conditions.

Parameters (in pu)	10% sag		20% sag		30% sag	
	Rectifier	Inverter	Rectifier	Inverter	Rectifier	Inverter
V_{DC}	0.8	0.8	0.7	0.7	0.5	0.5
I_{DC}	0.8	0.8	0.7	0.7	0.5	0.5
P at steady-state	0.75	0.7	0.63	0.6	0.52	0.5
Q at steady-state	−0.25	0.4	−0.1	0.8	−0.15	1

5.0.1. Sag Type-C

The type-C sag causes the dip in voltages and phase angles of the two phases, while the third phase is the reference phasor. The voltage expression and the phasor diagram of type-C sag are shown in Table 2. For the simulation analysis, the voltage dip in phases B and C are assumed to be 50%, and the phase angle shift is considered to be 140° in both phases. The impact of type-C sag on the performance of the FASAL system is shown in Fig. 12. The performance is measured in terms of 3-phase network voltage, stator current, rotor current, and active power of stator and rotor (i.e., P_1 and P_2). It is evident from Fig. 12(a) that before the

occurrence of sag, the stator current is balanced. However, after $t = 4.05$ s when sag appears in the network voltage, the 3-phase stator voltage and the current becomes unbalanced and distorted, as depicted in Fig. 12(b). Moreover, during dip, the distortion in rotor current is much more than the stator current as shown in Fig. 12(c). Furthermore, due to sag, the dip appears in the real power (Fig. 12(d)) and P_1 and P_2 reduce from nominal power, i.e., 190 MW and 230 MW to $P_1 = 120$ MW and $P_2 = 100$ MW. In this condition, a reduction in stator and rotor active power level is significantly high due to higher losses under sag condition.

Table 7
Comparative summary of both systems under unbalanced network conditions.

| S. No.	BTB VSC–HVDC link	FASAL	Inference
1.	At the beginning of the steady-state, the reactive power demand increases sharply (Fig. 7(e)). The dedicated control systems (Guo and Zhao, 2009) tackles this.	At steady-state, neither such reactive power demand is required, nor a control system is needed.	Reactive power requirement is high in VSC-HVDC.
2.	It does not have overload capability. A large transient current due to disturbances will stress or damage the valves (Du et al., 2007).	It has significant overload capability due to the presence of an electro-mechanical device and can withstand large transient current.	The overload capacity of the FASAL system is high in comparison to the VSC-HVDC system.
3.	The effect of symmetrical voltage dip on the real power transmission is given as: • For 10% sag the value of P_1 and P_2 are 0.75 pu and 0.70 pu. • For 20% sag the value of P_1 and P_2 are 0.63 pu and 0.60 pu. • For 30% sag the value of P_1 and P_2 are 0.52 pu and 0.50 pu.	The effect of symmetrical voltage dip on the real power transmission is given as: • For 10% sag the value of P_1 and P_2 are 0.95 pu and 0.85 pu. • For 20% sag the value of P_1 and P_2 are 0.78 pu and 0.65 pu. • For 30% sag the value of P_1 and P_2 are 0.60 pu and 0.53 pu.	Reduction in real power due to voltage sag is significantly high in BTB VSC-HVDC.
4.	There is reduction in the magnitude of DC voltage, current and real power whereas fluctuations and oscillations increase (Figs 8, 9 and 10).	The reduction in voltage, current, and real power is not very significant. Moreover, these fluctuations and oscillations in real power are also small (Fig. 5).	Fluctuations and oscillations in voltage, current, and real power are less in FASAL.
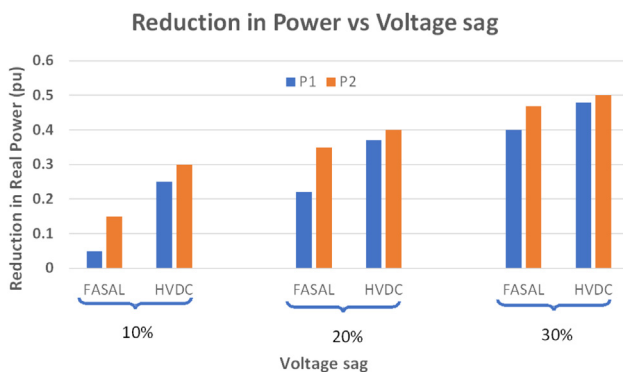
Fig. 11. Comparison of reduction in power corresponding to different sag condition for FASAL and HVDC.

5.0.2. Sag Type-D

In type-D sag, the voltage dip in one phase is significantly high, while the other two phases have the phase-angle shift and small voltage drop, which is demonstrated by the vector diagram in Table 2. A dip of 50% in phase A and 15% each in phase B and C at $t = 4.05$ s in the magnitude of network voltage is considered for simulation. Further, the unbalancing in the phase angle between A and B is 110° and, between phase B and C is 140°, as shown in Fig. 13(a).

The response of the FASAL system under type-D sag is shown in Fig. 13. Similar to the previous case, after the sag, the stator current becomes unbalanced and distorted, as shown in Fig. 13(b). The amplitude of current of each phase becomes different. Moreover, the rotor current waveform has severe distortion than the stator current, as shown in Fig. 13(c). Furthermore, the reduction in the stator and rotor real power are found as $P_1 = 143$ MW and $P_2 = 119$ MW (Fig. 13(d)).

It is evident that the influence of type-D sag on the real power is less as compared to type-C, but stator and rotor current has higher distortion levels than type-C and type-D. The rotor current of the DFIM under fault conditions is determined by taking the superposition of the positive, negative, and zero-sequence components. The maximum negative-sequence components in the network voltage are generated by the line-to-line faults. Therefore, the highest initial overshoot appears in the rotor current under sag types C and D compared to any other types of sag.

5.0.3. Sag Type-F

Here, the voltage dip in one phase is significantly higher than the other two phases, but the two phases also have a phase-angle shift described by the vector diagram in Table 2. The difference between the sag type-F and type-D is that the two phases in type-D have a smaller dip in voltage magnitude than type-F. The lowest magnitude for a type D sag is 86.60%, whereas, for a type F sag, it is 57.70% (Bollen, 2000). The simulation results are shown in Fig. 14 which include 3-phase network voltage, stator current, rotor currents, and stator and rotor active power. The parameters of type-F sag considered for the simulation are: 50% dip in voltage magnitude in phase A and 30% each in phase B and C. Like the previous case, this fault also occurs at $t = 4.05$ s with the phase angle unbalance as 110° between A and B and 140° between B and C is as shown in Fig. 14(a).

The effect of type-F sag on the FASAL system is shown in Fig. 14. It is evident from the plots of stator current (Fig. 14(b)), the rotor current (Fig. 14(c)), and their active power (Fig. 14(d)) that after the incident of type-F sag, the waveforms of these parameters gets unbalanced and distorted. The rotor current contains a moderate level of distortion than the previous two cases of asymmetric sag. The stator and rotor real power reduces to $P_1 = 103$ MW and $P_2 = 93$ MW, which shows that type-F sag causes a substantial reduction in power among all the other types of sag.
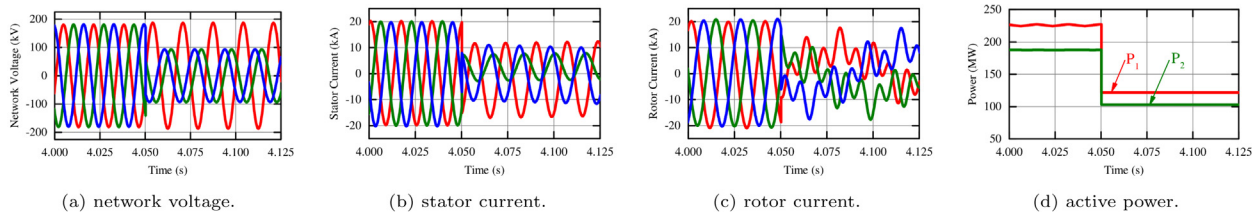
(a) network voltage.

(b) stator current.

(c) rotor current.

(d) active power.

Fig. 12. FASAL system performance under type-C sag condition.

(a) network voltage.

(b) stator current.

(c) rotor current.

(d) active power.
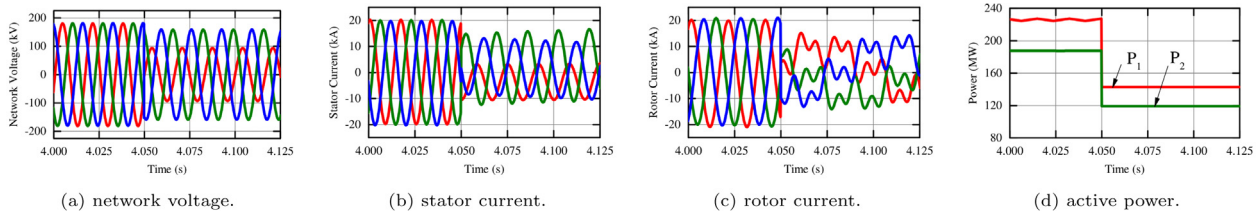
Fig. 13. FASAL system performance under type-D sag condition.

(a) network voltage.

(b) stator current.

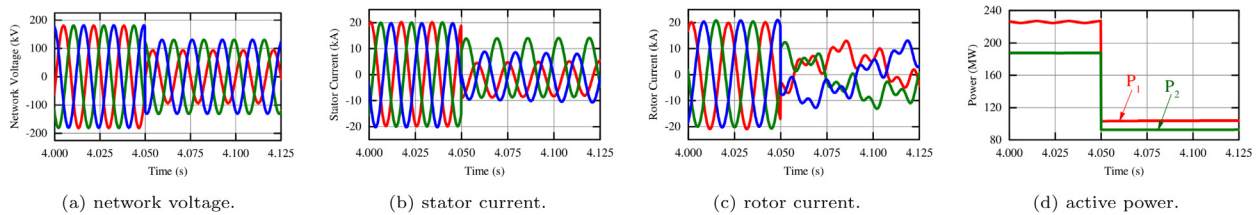(c) rotor current.

(d) active power.

Fig. 14. FASAL system performance under type-F sag condition.

Table 8
Comparison of asymmetrical sags for the FASAL.

Asymmetrical sags	Reduction in Power (pu)		Distortion in I_s & I_r
	P_1	P_2	
Type C	0.40	0.50	High
Type D	0.28	0.40	Medium
Type F	0.50	0.54	Moderate

Table 8 summarizes the performance of the FASAL system under asymmetrical sag conditions. It can be concluded from this table that the severity of power reduction is highest in type-F sag and lowest in type-C sag. Whereas the opposite is true in case of distortion in the stator and rotor current, i.e., type-C sag constitutes the highest distortion and unbalancing in I_s and I_r than type-D and F.

In short, this analysis helps in understanding the responses of the FASAL system at different voltage sag conditions. Based on these analyses, a researcher can propose suitable control schemes in future to tackle the problem of current distortion and power reduction.

6. Conclusion

In this paper, a detailed and comprehensive performance analysis of a newly developed FASAL system is investigated under various symmetrical and asymmetrical unbalanced grid voltage conditions. The simulation analysis is performed in PSCAD/EMTDC software environment to analyze the transient and steady-state responses in the stator current, rotor current, and real power under different sag types. Moreover, the performance of the FASAL system is also compared with the BTB VSC-HVDC link to substantiate its significance with the existing methodology. The results are compared for these two techniques which are as follows.

- It is observed that only four types of sag (type A, C, D, and F) reach to the terminals of the FASAL system for any fault. Therefore, the impact of these sags is only studied for the performance evaluation of the FASAL system.
- The reactive power requirement in the FASAL system is lesser than the BTB VSC-HVDC system because of less use of power electronics devices.
- The FASAL system, being built with an electromechanical device, can withstand high overloading than the BTB VSC-HVDC system.
- Under voltage sag conditions, a significant reduction in real power is found in BTB VSC-HVDC system than the FASAL system.
- The FASAL system exhibits lesser fluctuations and oscillations in voltage, current, and real power than the BTB VSC-HVDC system.

In addition to that, the simulation analysis presented in this paper provides a better understanding of the FASAL system under various sag conditions. In future work, the attempt will be made to analyze the performance of the FASAL system during overloading and underloading scenarios. Moreover, these results will also help in designing a suitable control scheme for the FASAL system to ride through the grid faults, unbalanced network, overloading, or underloading conditions.

CRediT authorship contribution statement

Imdadullah: Conceptualization, Validation, Simulation programming, Writing - original draft, Writing - review & editing. **Syed Muhammad Amrr:** Formal analysis, Writing - review & editing. **Atif Iqbal:** Funding acquisition, Proofreading. **M.S. Jamil Asghar:** Supervision, Conceptualization, Methodology, Writing - review & editing.

Declaration of competing interest

References

Ambati, B.B., Kanjiya, P., Khadkikar, V., El Moursi, M.S., Kirtley, J.L., 2015. A hierarchical control strategy with fault ride-through capability for variable frequency transformer. IEEE Trans. Energy Convers. 30 (1), 132–141.

Asghar, M.J., Imdadullah, 2018. A flexible asynchronous ac link (FASAL) system. Google Patents, Indian Patent 296524.

Bollen, M.H., 2000. Understanding Power Quality Problems: Voltage Sags and Interruptions. IEEE Press.

Chen, S., Lu, J., Zhang, G., Zhang, Y., 2020. Immunizing variable frequency transformer from dual-side asymmetrical grid faults via a single-converter-based novel control strategy. IEEE Trans. Power Deliv. 35 (3), 1330–1338.

Du, C., Bollen, M.H., Agneholm, E., Sannino, A., 2007. A new control strategy of a VSC–HVDC system for high-quality supply of industrial plants. IEEE Trans. Power Deliv. 22 (4), 2386–2394.

Dugan, R.C., McGranaghan, M.F., Beaty, H.W., 1996. Electrical Power Systems Quality. McGraw-Hill, New York.

Dusseault, M., Gagnon, J., Galibois, D., Granger, M., McNabb, D., Nadeau, D., Primeau, J., Fiset, S., Larsen, E., Drobniak, G., et al., 2004. First VFT application and commissioning. Canada Power 28–30.

Fallah, M., Kojabadi, H.M., Blaabjerg, F., 2020. New control method for VSC-MTDC stations in the abnormal conditions of power system. Control Eng. Pract. 96, 104316.

Gomis-Bellmunt, O., Junyent-Ferre, A., Sumper, A., Bergas-Jane, J., 2008. Ride-through control of a doubly fed induction generator under unbalanced voltage sags. IEEE Trans. Energy Convers. 23 (4), 1036–1045.

Guo, C., Zhang, Y., Gole, A.M., Zhao, C., 2012. Analysis of dual-infeed HVDC with LCC–HVDC and VSC–HVDC. IEEE Trans. Power Deliv. 27 (3), 1529–1537.

Guo, C., Zhao, C., 2009. A new technology for HVDC start-up and operation using VSC-HVDC system. In: Proc. IEEE Power Energy Soc. Gen. Meet., pp. 1–5.

Han, Y., Feng, Y., Yang, P., Xu, L., Xu, Y., Blaabjerg, F., 2020. Cause, classification of voltage sag, and voltage sag emulators and applications: A comprehensive overview. IEEE Access 8, 1922–1934.

Hao, Q., Li, D., Li, B., Wang, S., 2020. Operation and control of MMC station with constraints of internal variables under unbalanced grid conditions. IET Gener. Transm. Distrib. 14 (10), 1829–1841.

Imdadullah, Amrr, S.M., Jamil Asghar, M.S., Ashraf, I., Meraj, M., 2020a. A comprehensive review of power flow controllers in interconnected power system networks. IEEE Access 8, 18036–18063. http://dx.doi.org/10.1109/access.2020.2968461.

Imdadullah, Asghar, M.S.J., 2019. Performance evaluation of doubly fed induction machine used in flexible asynchronous AC link for power flow control applications. In: 2019 Int. Conf. on Electrical, Electronics and Computer Engineering. pp. 1–6. http://dx.doi.org/10.1109/UPCON47278.2019.8980227.

Imdadullah, Beig, A.R., Asghar, M.S.J., 2020b. Performance evaluation and reliability of flexible asynchronous ac link and LCC-HVDC link under fault conditions. IEEE Access 8, 120562–120574.

Imdadullah, Rahman, H., Asghar, M.S.J., 2019. A flexible asynchronous AC link for two area power system networks. IEEE Trans. Power Deliv. 34 (5), 2039–2049.

Ismail, A.G., El-Dabah, M.A., Nassar, I.A., 2020. Enhancement of electrical distribution networks performance using the load management methodology. Energy Rep. 6, 2066–2074.

Jiang, F., Tu, C., Guo, Q., Shuai, Z., He, X., He, J., 2019. Dual-functional dynamic voltage restorer to limit fault current. IEEE Trans. Ind. Electron. 66 (7), 5300–5309.

Kang, T., Choi, S., Morsy, A.S., Enjeti, P.N., 2017. Series voltage regulator for a distribution transformer to compensate voltage sag/swell. IEEE Trans. Ind. Electron. 64 (6), 4501–4510.

Lim, P.K., Dorr, D.S., 2000. Understanding and resolving voltage sag related problems for sensitive industrial customers. In: Proc. IEEE Power Eng. Soc. Winter Meeting, vol. 4, pp. 2886–2890.

Liu, T., Jiang, M., Zhang, D., Zhao, H., Shuang, F., 2020. Effect of symmetrical voltage sag on induction motor considering phase-angle factors based on a new 2-D multi-slice time-stepping finite element method. IEEE Access 8, 75946–75956.

Liu, W., Zheng, T., Liu, Z., Fan, Z., Kang, Y., Wang, D., Zhang, M., Miao, S., 2018. Active and reactive power compensation control strategy for VSC-HVDC systems under unbalanced grid conditions. Energies 11 (11), 3140.

Marken, P., Roedel, J., Nadeau, D., Wallace, D., Mongeau, H., 2008. VFT maintenance and operating performance. In: IEEE Power and Energy Society General Meeting-Conversion and Delivery of Electrical Energy in the 21st Century, pp. 1–5.

Merkhouf, A., Doyon, P., Upadhyay, S., 2008. Variable frequency transformer–Concept and electromagnetic design evaluation. IEEE Trans. Energy Convers. 23 (4), 989–996.

Mohseni, M., Islam, S.M., Masoum, M.A.S., 2011. Impacts of symmetrical and asymmetrical voltage sags on DFIG-based wind turbines considering phase-angle jump, voltage recovery, and sag parameters. IEEE Trans. Power Electron. 26 (5), 1587–1598. http://dx.doi.org/10.1109/TPEL.2010.2087771.

Omara, M.A., Nassar, I.A., 2019. Voltage quality in delta Egypt network and its impact in oil industry. Energy Rep. 5, 29–36.

Plihal, K., Do, A., Deleanu, S., Andrei, H., Stanculescu, M., Iordache, M., 2019. A study on the implementation of HVDC for Power system interconnection. In: 6th IEEE International Symposium on Electrical and Electronics Engineering, pp. 1–6.

Rodriguez, P., Timbus, A.V., Teodorescu, R., Liserre, M., Blaabjerg, F., 2007. Flexible active power control of distributed power generation systems during grid faults. IEEE Trans. Ind. Electron, 54 (5), 2583–2592.

Saeedifard, M., Iravani, R., 2010. Dynamic performance of a modular multilevel back-to-back HVDC system. IEEE Trans. Power Deliv. 25 (4), 2903–2912.

Saeedifard, M., Iravani, R., Pou, J., 2009. A space vector modulation strategy for a back-to-back five–level HVDC converter system. IEEE Trans. Ind. Electron. 56 (2), 452–466.

Shi, X., Filizadeh, S., 2019. Independent-phase current control of a three-phase VSC under unbalanced operating conditions. J. Eng. 2019 (16), 1338–1345.

Somayajula, D., Crow, M.L., 2015. An integrated dynamic voltage restorer-ultracapacitor design for improving power quality of the distribution grid. IEEE Trans. Sustain. Energy 6 (2), 616–624.

Tang, X., Zhan, R., Xi, Y., Xu, X., 2019. Resonance investigation and active damping method for VSC-HVDC transmission systems under unbalanced faults. J. Power Electron. 19 (6), 1467–1476.

Tu, C., Guo, Q., Jiang, F., Wang, H., Shuai, Z., 2019. A comprehensive study to mitigate voltage sags and phase jumps using a dynamic voltage restorer. IEEE J. Emerg. Sel. Topics Power Electron. 8 (2), 1490–1502.

Ufa, R., Gusev, A., Diab, A.A.Z., Suvorov, A., Ruban, N., Andreev, M., Askarov, A., Rudnik, V., Abdalla, O., Ali, Z.M., et al., 2020. Analysis of application of back-to-back HVDC system in tomsk electric power system. Energy Rep. 6, 438–444.

Von Jouanne, A., Banerjee, B., 2001. Assessment of voltage unbalance. IEEE Trans. Power Deliv. 16 (4), 782–790.

Wang, S., Dragicevic, T., Gao, Y., Chaudhary, S., Teodorescu, R., 2020. Machine learning based operating region extension of modular multilevel converters under unbalanced grid faults. IEEE Trans. Ind. Electron..

Wei, X., Tang, G., 2006. Analysis and control VSC-HVDC under unbalanced AC conditions. In: IEEE International Conference on Power System Technology, pp. 1–5.

Wen, Y., Chung, C.Y., Ye, X., 2018. Enhancing frequency stability of asynchronous grids interconnected with HVDC links. IEEE Trans. Power Syst. 33 (2), 1800–1810.

Xu, D., Blaabjerg, F., Chen, W., Zhu, N., 2018. Advanced Control of Doubly Fed Induction Generator for Wind Power Systems. John Wiley & Sons.